Dynamics of prolate ellipsoidal particles in a turbulent channel flow

P. H. Mortensen,[1] H. I. Andersson,[1] J. J. J. Gillissen,[2] and B. J. Boersma[2]
[1]*Department of Energy and Process Engineering, Norwegian University of Science and Technology, 7491 Trondheim, Norway*
[2]*Laboratory for Aero and Hydrodynamics, TU-Delft, 2628 CA Delft, The Netherlands*

(Received 11 January 2008; accepted 13 June 2008; published online 9 September 2008)

The dynamical behavior of tiny elongated particles in a directly simulated turbulent flow field is investigated. The ellipsoidal particles are affected both by inertia and hydrodynamic forces and torques. The time evolution of the particle orientation and translational and rotational motions in a statistically steady channel flow is obtained for six different particle classes. The focus is on the influence of particle aspect ratio λ and the particle response time on the particle dynamics, i.e., distribution, orientation, translation, and rotation. Both ellipsoidal and spherical particles tend to accumulate in the viscous sublayer and preferentially concentrate in regions of low-speed fluid velocity. The translational motion is practically unaffected by the aspect ratio, whereas both mean and fluctuating spin components depend crucially on λ. The ellipsoids tend to align themselves with the mean flow direction and this tendency becomes more pronounced in the wall proximity when the lateral tilting of the elongated particles is suppressed. © *2008 American Institute of Physics*.
[DOI: 10.1063/1.2975209]

I. INTRODUCTION

The motions of small elongated particles in a turbulent background flow are of both industrial and environmental importance, as well as of academical and fundamental interest. Suspensions of elongated particles occur in several natural and industrial applications, such as aerosols in the atmosphere, meteorology, paper industry, combustion processes, and pneumatic transport, to name a few. Hence, it is of vital importance to have a clear understanding of such flow suspensions. It is believed that direct numerical simulations (DNS) will provide a better insight to the problem, and as a consequence, give some impact on the modeling part of dispersed multiphase flows. The motion of nonspherical particles in turbulent shear flows is intriguingly complicated. Most of the literature on particulate fluid flows reports the fluid interactions with spherical particles (see, for example, Refs. 1–7). Spherical particles are mathematically simpler to treat than nonspherical particles because of their isotropic nature, i.e., every axis through the spherical mass center is a principal axis. However, a nonspherical particle which possesses anisotropic nature is by far more complicated to treat. First of all, the nonspherical shape causes a coupling between the linear and angular momenta due to the particle orientation.

The study of elongated particles suspended in viscous fluid flows has been a topic for research through many decades. Jeffery[8] studied an ellipsoidal particle immersed in creeping viscous fluid. He analytically derived the torque components acting along the ellipsoids principal axes. Further analytical work on particles of different geometrical shapes has been conducted by Brenner[9–13] and Happel and Brenner.[14] Also, Harper and Chang[15] calculated the lift tensor for an arbitrary three-dimensional body in a low Reynolds number shear flow by asymptotic methods. All these different analytical studies assume Stokes flow conditions around the particles, i.e., viscous effects dominate over inertial effects. Lin *et al.*[16] nicely summarized the work related to nonspherical particles in laminar shear flows and sedimentation of nonspherical particles in still fluids.

Not that many numerical and experimental studies have been devoted to nonspherical particles in turbulent flows. As is the case, the motion of nonspherical particles even in laminar flows is rather complicated. A turbulent background flow makes this problem even more intriguing. Some works on nonspherical particles have focused on the motion of ellipsoidal particles and fibers in homogeneous isotropic turbulence, like Fan and Ahmadi[17] and Olson.[18] Attention has also been devoted to the deposition process of nonspherical and ellipsoidal particles. Shapiro and Goldenberg[19] experimentally investigated the deposition of glass fibers in a turbulent pipe flow. Fan and Ahmadi[20,21] numerically studied the deposition of ellipsoidal particles in a wall-bounded turbulent flow. Zhang *et al.*[22] investigated by means of DNS the transport and deposition of ellipsoidal particles in a turbulent channel flow. They provided velocity and orientational particle statistics in the near-wall regions (i.e., viscous sublayer and buffer layer). Some investigations have also focused on the orientation of nonspherical particles in turbulent flows. Klett[23] proposed a model for the orientation of particles in turbulence. He assumed that the particles were subjected to isotropic turbulence within or below the inertial subrange. Newsom and Bruce[24] experimentally and numerically investigated the orientational properties of aerosols in the atmospheric turbulent boundary layer. Their experiments showed that the particles' mean orientation was in the horizontal direction. The model, however, overestimated the observed mean orientation. Lin *et al.*[25] performed numerical studies on the orientation distribution of fibers immersed in laminar and turbulent pipe flows. They reported that, in the laminar regime, the fibers were more aligned in the flow direction with

increasing Reynolds number. In the turbulent regime, the orientational distribution became more homogeneous with increasing Reynolds number.

An alternative approach to fluid-fiber interactions is based on a statistical description of an ensemble of fibers, (see, for instance, Refs. 26–28). In these studies, the fibers are assumed to be inertia-free, and the fiber effect on the solvent results in an extra stress term in the Navier–Stokes equations. These methods are used to study particle-induced drag reduction in turbulent flows.

In the present paper, the dynamics of small prolate ellipsoidal particles in a turbulent channel flow is investigated by means of DNS. While the Eulerian approach is adopted for the turbulence field, the nonspherical particles are treated in a Lagrangian framework. The focus is on the translational and rotational particle motions and the influence of particles on the turbulence is therefore neglected. Further, where it is convenient, the ellipsoidal particle data are compared to its spherical counterpart. Since the translational and rotational motions of an ellipsoidal particle cannot be solved independently, the nine direction cosines must be calculated for the particle orientation. Usually these parameters are comprised by the three independent Euler angles (see Ref. 29). However, the Euler angles suffer from singularity problems. For this reason, the corresponding four Euler parameters will be used for the particle orientation. In order to keep the study simple, the particles are only subjected to hydrodynamic drag force[12] and torque.[8]

The present approach is analogous to that taken by Zhang *et al.*,[22] but their focus was on particle deposition. This paper is an extension of previous work by Mortensen *et al.*,[30] where only a modest number of prolate ellipsoids were investigated on a relatively coarse computational mesh. Here, a much finer grid is adopted for the DNS and the number of particles have increased significantly. In addition, the present computational domain is substantially larger than that used by Zhang *et al.*[22] Also, Zhang *et al.*[22] showed velocity and orientational statistics for particles of aspect ratio $\lambda=5$ and equivalent response time $\tau^+=5$ in the near-wall region (viscous sublayer, buffer layer). The forces acting on the particles were the hydrodynamic drag, shear-induced lift, and gravity. In the present paper, a broader particle parameter space is investigated, and particle statistics is reported for the whole cross section. Also, the only acting force on the particles is the hydrodynamic drag force.

The outline of the paper is as follows. Sections II and III deal with theory and simulations of the fluid and particles, respectively. Section IV comprises results and discussions. Here, particle distribution profiles, velocity, and orientational statistics will be presented. Finally, Sec. V summarizes and concludes the work.

II. EULERIAN FLUID DYNAMICS

The incompressible, isothermal, and Newtonian fluid into which the particles are released is governed by the continuity and the Navier–Stokes equation,

$$\nabla \cdot \mathbf{u} = 0, \tag{1}$$

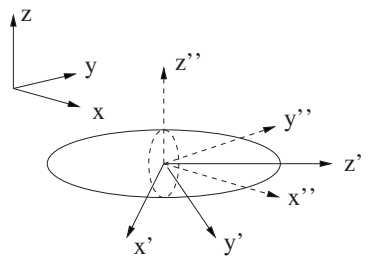

FIG. 1. Cartesian coordinate systems; inertial frame $\mathbf{x}$, particle frame $\mathbf{x}'$, and comoving frame $\mathbf{x}''$.

$$\frac{\partial \mathbf{u}}{\partial t} + (\mathbf{u} \cdot \nabla)\mathbf{u} = -\nabla p + \mathrm{Re}_*^{-1}\nabla^2\mathbf{u}. \tag{2}$$

In the equations above, $\mathbf{u}=\langle u_x, u_y, u_z\rangle$ is the fluid velocity vector in the Cartesian reference frame $\mathbf{x}=\langle x, y, z\rangle$, p is the pressure, and $\mathrm{Re}_*=u_* h/\nu$ is the frictional Reynolds number. Here, $\mathbf{u}$ and $\mathbf{x}$ are scaled with the friction velocity u_* and the channel height h, respectively, while the time is scaled with h/u_*. The kinematic fluid viscosity is denoted by ν.

A DNS is used to solve the fluid equations of motion [Eqs. (1) and (2)] at a frictional Reynolds number $\mathrm{Re}_*=360$, whereas Zhang *et al.*[22] considered the somewhat lower $\mathrm{Re}_*=250$. The size of the computational domain is $6h$ in the streamwise direction, $3h$ in the spanwise direction, and h in the wall-normal direction. This domain size, which is three times longer and 50% wider than that used by Zhang *et al.*,[22] is considered as appropriate for channel flow simulations. Periodic boundary conditions are applied in the streamwise (x) and spanwise (y) directions. In the wall-normal direction (z), no-slip conditions are enforced at both walls ($z=0$ and $z=h$). The computations are carried out with $192\times192\times192$ gridpoints in the x, y, and z directions, respectively. In the wall-normal direction the grid is slightly refined toward the wall such that Δz^+ varies between 0.9 and 2.86. The resolutions in the streamwise and spanwise directions are $\Delta x^+=11.3$ and $\Delta y^+=5.6$, respectively. The timestep is $\Delta t^+=0.036$ in wall units. The same algorithm as that used by Gillissen *et al.*[28] is employed for solving the fluid equations of motion.

III. LAGRANGIAN PARTICLE DYNAMICS

In order to describe the general motion of prolate ellipsoids, it is convenient to invoke three different Cartesian coordinate systems: the inertial frame, the particle frame, and the comoving frame. The inertial frame, $\mathbf{x}=\langle x, y, z\rangle$, is the frame that spans the computational domain. The particle frame, $\mathbf{x}'=\langle x', y', z'\rangle$, is attached to the particle with its origin at the particle mass center. The coordinate axes are aligned with the principal directions of inertia. The comoving frame, $\mathbf{x}''=\langle x'', y'', z''\rangle$, is attached to the particle with its origin at the mass center of the particle. The coordinate axes are parallel to those of the inertial frame. The different coordinate systems are shown in Fig. 1. The purpose of introducing the comoving system is to describe the orientational behavior of the ellipsoids. The particle orientation is important since it influences both the rotational and translational mo-

tions. The orientation of the particle frame relative to the comoving frame is given by the nine direction cosines[29] which relate the same vector in two different coordinate systems through the linear transformation $\mathbf{x}'=\mathbf{A}\mathbf{x}''$. The orthogonal transformation matrix $\mathbf{A}$ comprises the direction cosines and is given by

$$\mathbf{A}=\begin{pmatrix} a_{11} & a_{12} & a_{13} \\ a_{21} & a_{22} & a_{23} \\ a_{31} & a_{32} & a_{33} \end{pmatrix}, \tag{3}$$

where the direction cosines a_{ij} are

$$a_{11}=e_0^2+e_1^2-e_2^2-e_3^2, \quad a_{12}=2(e_1e_2+e_0e_3),$$

$$a_{13}=2(e_1e_3-e_0e_2), \quad a_{21}=2(e_1e_2-e_0e_3),$$

$$a_{22}=e_0^2-e_1^2+e_2^2-e_3^2, \quad a_{23}=2(e_2e_3+e_0e_1),$$

$$a_{31}=2(e_1e_3+e_0e_2), \quad a_{32}=2(e_2e_3-e_0e_1),$$

$$a_{33}=e_0^2-e_1^2-e_2^2+e_3^2.$$

The parameters e_0, e_1, e_2, and e_3 are the Euler parameters. These parameters are dependent and must satisfy the following constraint:

$$e_0^2+e_1^2+e_2^2+e_3^2=1. \tag{4}$$

The translational equation of motion of an individual particle is given by the linear momentum relation according to

$$m\frac{d\mathbf{v}}{dt}=\mathbf{F}. \tag{5}$$

Here, m is mass of the ellipsoid and $\mathbf{v}=\langle v_x,v_y,v_z\rangle$ is the particle velocity vector. The drag force $\mathbf{F}$, acting on an ellipsoid under creeping flow conditions, is given by[12]

$$\mathbf{F}=\mu\mathbf{A}'\mathbf{K}'\mathbf{A}(\mathbf{u}-\mathbf{v}), \tag{6}$$

where $\mu=\rho\nu$ is the dynamic viscosity of the fluid. For an ellipse of revolution about the z'-axis, the resistance tensor $\mathbf{K}'$ is

$$\mathbf{K}'=\begin{pmatrix} k'_{xx} & 0 & 0 \\ 0 & k'_{yy} & 0 \\ 0 & 0 & k'_{zz} \end{pmatrix}, \tag{7}$$

where k'_{xx}, k'_{yy}, and k'_{zz} are the components along the x', y', and z' axes (principal directions), respectively, and are given as[31]

$$k'_{xx}=k'_{yy}=\frac{16\pi a(\lambda^2-1)^{3/2}}{(2\lambda-3)\ln[\lambda+(\lambda^2-1)^{1/2}]+\lambda(\lambda^2-1)^{1/2}}, \tag{8}$$

$$k'_{zz}=\frac{8\pi a(\lambda^2-1)^{3/2}}{(2\lambda-1)\ln[\lambda+(\lambda^2-1)^{1/2}]+\lambda(\lambda^2-1)^{1/2}}. \tag{9}$$

In Eqs. (8) and (9), the aspect ratio $\lambda=b/a$ where a is the semiminor axis and b is the semimajor axis of the ellipsoid. These expressions are valid for prolate ellipsoids ($\lambda>1$).

The particle translational displacement is given by

$$\mathbf{x}=\int \mathbf{v}dt. \tag{10}$$

An important parameter is the particle response time, i.e., the time the particle needs to respond to changes in the local flow field due to its inertia. For an ellipsoidal particle which is nonisotropic, the response time is not as obvious as for a spherical particle. Shapiro and Goldenberg[19] defined an equivalent response time based on isotropic particle orientation and the inverse of the resistance tensor. Zhang *et al.*[22] presented their result in the form

$$\tau^+=\frac{2\lambda Da^{+2}}{9}\frac{\ln(\lambda+\sqrt{\lambda^2-1})}{\sqrt{\lambda^2-1}}, \tag{11}$$

where the particle equivalent response time τ is scaled with the viscous time scale ν/u_*^2 and D is the density ratio between the particle and the fluid.

The rotational motion of the ellipsoids is given by the Euler equations,[29]

$$I'_{xx}\frac{d\omega'_x}{dt}-\omega'_y\omega'_z(I'_{yy}-I'_{zz})=N'_x, \tag{12}$$

$$I'_{yy}\frac{d\omega'_y}{dt}-\omega'_z\omega'_x(I'_{zz}-I'_{xx})=N'_y, \tag{13}$$

$$I'_{zz}\frac{d\omega'_z}{dt}-\omega'_x\omega'_y(I'_{xx}-I'_{yy})=N'_z, \tag{14}$$

where ω'_x, ω'_y, and ω'_z are the components of the angular velocity vector. Notice that the Euler equations are formulated in the particle frame. The principal moments of inertia are

$$I'_{xx}=I'_{yy}=\frac{(1+\lambda^2)ma^2}{5}, \quad I'_{zz}=\frac{2ma^2}{5}. \tag{15}$$

The torque components (N'_x, N'_y, N'_z) were derived by Jeffery[8] for an ellipsoid subjected to linear shear under creeping flow conditions and are given as

$$N'_x=\frac{16\pi\mu a^3\lambda}{3(\beta_0+\lambda^2\gamma_0)}[(1-\lambda^2)f'+(1+\lambda^2)(\xi'-\omega'_x)], \tag{16}$$

$$N'_y=\frac{16\pi\mu a^3\lambda}{3(\lambda^2\gamma_0+\alpha_0)}[(\lambda^2-1)g'+(\lambda^2+1)(\eta'-\omega'_y)], \tag{17}$$

$$N'_z=\frac{32\pi\mu a^3\lambda}{3(\alpha_0+\beta_0)}(\chi'-\omega'_z), \tag{18}$$

where f' and g' are the fluid rates of strain coefficients,

$$f'=\tfrac{1}{2}(u'_{z,y}+u'_{y,z}), \tag{19}$$

$$g'=\tfrac{1}{2}(u'_{x,z}+u'_{z,x}), \tag{20}$$

and ξ', η', and χ' are the fluid rotation rate coefficients,

$$\xi'=\tfrac{1}{2}(u'_{z,y}-u'_{y,z}), \tag{21}$$

$$\eta'=\tfrac{1}{2}(u'_{x,z}-u'_{z,x}), \tag{22}$$

$$\chi' = \tfrac{1}{2}(u'_{x,y} - u'_{y,x}). \tag{23}$$

These coefficients are half of the fluid vorticity $\mathbf{\Omega}'$ expressed in the particle frame. The parameters α_0, β_0, and γ_0 in the expressions [(16)–(18)] for the torque components are[31]

$$\alpha_0 = \beta_0 = \frac{2\lambda^2(\lambda^2-1)^{1/2} + \lambda \ln\left[\dfrac{\lambda - (\lambda^2-1)^{1/2}}{\lambda + (\lambda^2-1)^{1/2}}\right]}{2(\lambda^2-1)^{3/2}}, \tag{24}$$

$$\gamma_0 = \frac{2(\lambda^2-1)^{1/2} + \lambda \ln\left[\dfrac{\lambda - (\lambda^2-1)^{1/2}}{\lambda + (\lambda^2-1)^{1/2}}\right]}{(\lambda^2-1)^{3/2}}. \tag{25}$$

The time rate of change of the Euler parameters is related to the particle angular velocities and is given as

$$\begin{pmatrix} \dot{e}_0 \\ \dot{e}_1 \\ \dot{e}_2 \\ \dot{e}_3 \end{pmatrix} = \frac{1}{2}\begin{pmatrix} e_0 & -e_1 & -e_2 & -e_3 \\ e_1 & e_0 & -e_3 & e_2 \\ e_2 & e_3 & e_0 & -e_1 \\ e_3 & -e_2 & e_1 & e_0 \end{pmatrix}\begin{pmatrix} 0 \\ \omega'_x \\ \omega'_y \\ \omega'_z \end{pmatrix}. \tag{26}$$

The particle translational and rotational equations of motion [Eqs. (5) and (12)–(14)] are solved by a mixed differencing procedure.[21] Equations (10) and (26) are solved by a second-order Adams–Bashforth scheme. Since the constraint (4) should be preserved in time, the Euler parameters are renormalized after every timestep in order to avoid accumulation of numerical errors.[32] For each particle at each timestep, the Euler parameters e_i are calculated from Eq. (26), where $i=0,3$ refers to the ith Euler parameter. The Euler parameters are then renormalized according to

$$e_i = \frac{e_i}{\sqrt{e_0^2 + e_1^2 + e_2^2 + e_3^2}}, \tag{27}$$

which will guarantee that the sum of the squares for each particle [Eq. (4)] is unity. If the Euler parameters are not renormalized $|\cos\theta|$ might occasionally exceed unity due to numerical errors (θ is one of the three Euler angles; see Ref. 29).

A second-order quadratic interpolation scheme is used for interpolation of the fluid variables at the particle positions. The timestep used during the integration of the particle equations is the same as that used for the Navier–Stokes equations. The particle boundary conditions are periodic in the two homogeneous directions. If a particle hits the wall, it is elastically bounced off the wall while keeping its previous linear momentum in the homogeneous directions and angular momentum. This is a rather crude wall model, but it is expected that the total number of wall collisions is not sufficiently frequent to significantly alter the particle statistics. On the other hand, a more realistic wall model for ellipsoids are not readily available. Another point to be addressed is that slip correction factors are not included in the particle equations of motion. For spherical particles, the drag correction factor often reads

TABLE I. Particle parameters for the six different cases.

Case	λ	D	τ^+
F1	1	173.6	5
F3	3	92.9	5
F10	10	57.7	5
S1	1	1041.7	30
S3	3	557.1	30
S10	10	346.3	30

$$C_D = \frac{24}{\mathrm{Re}_p}(1 + 0.15\,\mathrm{Re}_p^{0.687}), \quad 0 < \mathrm{Re}_p < 1000, \tag{28}$$

where Re_p is the particle Reynolds number based on the particle relative velocity and particle diameter. However, no such correction factors have been presented for ellipsoidal particles. In order to make comparisons between spheres ($\lambda = 1$) and ellipsoids ($\lambda > 1$), Eq. (28) is not included in the spherical particle equation of motion. It should also be noted that wall-correction factors are not included in present study. Arcen *et al.*[33] showed that wall-correction forces (drag and lift) have negligible effect on the statistics of spherical particles for response times of the order considered in the present paper.

IV. RESULTS AND DISCUSSION

The present paper will focus on the distribution and velocity statistics of small inertial prolate ellipsoidal particles in a turbulent channel flow. Also, the orientation of the ellipsoids will be reported and discussed. The objective is to report the effect of varying the particle equivalent response time and aspect ratio on the instantaneous particle distribution, velocity statistics, and orientation. For the investigation of the particle dynamics, six different particle cases are studied; see Table I. In all cases, the number of particles N and the particle semiminor axis a is kept constant. By varying the density ratio D and the aspect ratio λ, the particle equivalent response time (11) is determined. We intentionally consider both fast (F) and slow (S) particles with response times τ^+ equal to 5 and 30, respectively. Some statistics for the spherical particles, i.e., cases F1 and S1, have already been reported by Mortensen *et al.*[34] Here, all six particle cases, each case consisting of $N=1\,000\,000$ particles, are treated in the same turbulence flow field.

The aim of this work is to explore the behavior of ellipsoidal particles in a turbulent shear flow. In reality, the flow field will also be affected by the presence of the particles. This latter effect depends on a number of parameters, notably the particle response time τ^+ defined in Eq. (11) and the particle loading. The flow of dilute suspensions of fast particles is practically unaffected by the presence of the particles, whereas the fluid motion is increasingly influenced by higher loading of slower particles. Such two-way coupled systems are certainly of fundamental and practical importance (see, e.g., Ref. 35) but are beyond the scope of the present study. The large number of particles ($N=10^6$) used herein was chosen in order to improve the particle statistics

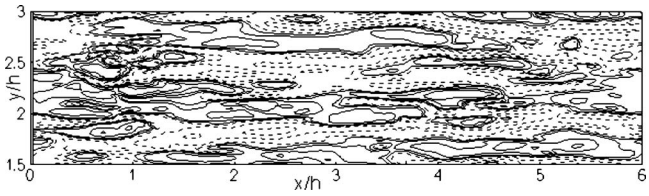

FIG. 2. Instantaneous contours of fluctuating streamwise fluid velocity at the plane $z^+=6.4$. The solid lines are positive and the dashed lines are negative fluctuations.

rather than to increase the particle loading. Equivalently smooth particle statistics could alternatively have been obtained with a much smaller number of particles, say $N=10^4$, in a 100 times longer simulation.

The results in Figs. 2–10 are instantaneous results at time $t^+=5760$, while the rest of the results are statistics averaged in time from $t^+=2880$ to $t^+=5760$. In Figs. 18–25 the particle spin is referred to the comoving frame $\mathbf{x}''$, i.e., $\boldsymbol{\omega}''=\mathbf{A}^{-1}\boldsymbol{\omega}'$.

A. Instantaneous particle distribution

The instantaneous contour plots and particle distribution presented in this section, i.e., Figs. 2–10, are typical samples and consistent with the conditional averages presented in Secs. IV B and IV C.

In wall-bounded turbulence, it is a well-known fact that particles accumulate in the near-wall region and has been observed and analyzed by several researchers (see, for example, Refs. 3, 4, 6, 7, 22, 36, and 37. It is a general consensus that particle accumulation is dependent on particle inertia and that the near-wall sweep and ejection events are highly correlated with the particle wall-normal convection. Still, there are open questions regarding the net transport of particles toward the walls. Marchioli and Soldati[6] attributed

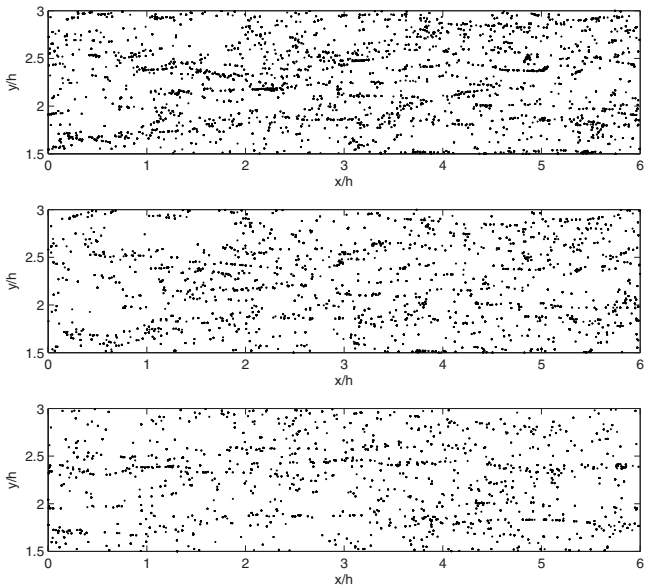

FIG. 3. Instantaneous distribution of particles around plane $z^+=6.4$ for particles of response time $\tau^+=5$. $\lambda=1$ (upper), $\lambda=3$ (middle), and $\lambda=10$ (lower).

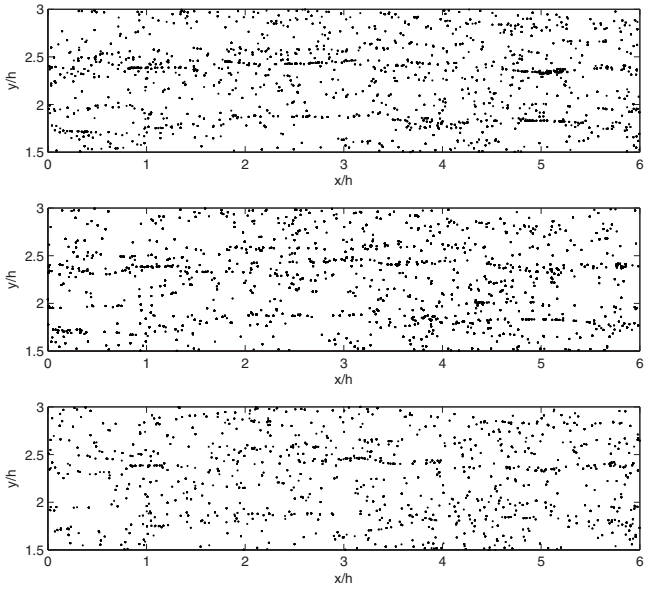

FIG. 4. Instantaneous distribution of particles around plane $z^+=6.4$ for particles of response time $\tau^+=30$. $\lambda=1$ (upper), $\lambda=3$ (middle), and $\lambda=10$ (lower).

this effect to the existence of primary and secondary quasistreamwise vortices in the turbulent boundary layer. The effect of secondary streamwise vortices, which arise in the wake of primary vortices, is to narrow the ejection zones. Hence, the result is a net transfer of particles toward the walls. Also Zhang *et al.*[22] proposed that, if a particle is trapped in the viscosity-dominated sublayer, it will experience a large residence time in this region due to the weak wall-normal turbulent fluctuations.

Figure 2 shows an instantaneous ($t^+=5760$) contour plot of streamwise fluid velocity fluctuations in the *xy*-plane at $z^+=6.4$. The dashed lines show negative velocity fluctuations and are commonly termed low-speed streaks. These low-speed streaks are features of the pulsating turbulent boundary layer and exist due to vortical structures, see Ref. 38. Along with Fig. 2 are Figs. 3 and 4, which show the distribution of particles with response times $\tau^+=5$ and $\tau^+=30$ around the same plane, respectively. It is seen that fast ($\tau^+=5$) and slow ($\tau^+=30$) particles preferentially concentrated along narrow regions which correspond to the low-speed regions in Fig. 2. This exiting feature has been observed both experimentally and numerically for spherical particles (see, for instance, Refs. 39 and 6). Eaton and Fessler[39] proposed that particles

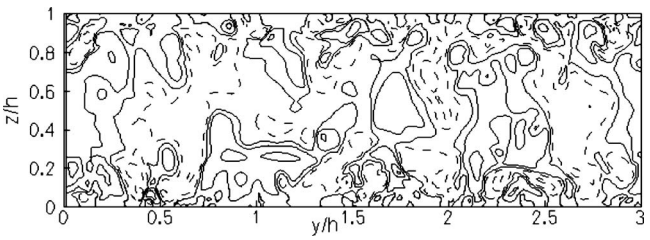

FIG. 5. Instantaneous contours of wall-normal fluid velocity at the plane $x^+=720$. The solid lines are positive and the dashed lines are negative velocity.

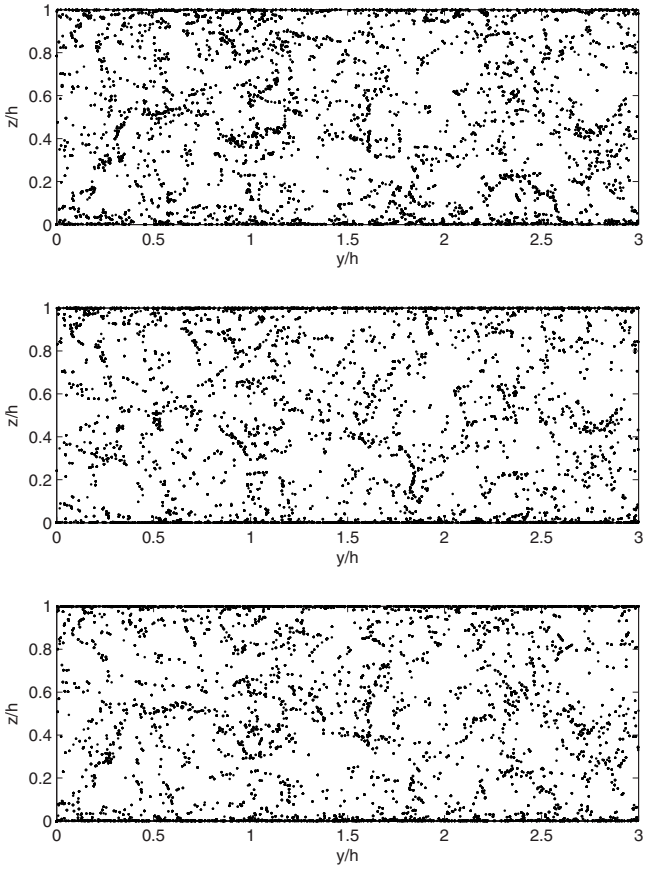

FIG. 6. Instantaneous distribution of particles around plane $x^+=720$ for particles of response time $\tau^+=5$. $\lambda=1$ (upper), $\lambda=3$ (middle), and $\lambda=10$ (lower).

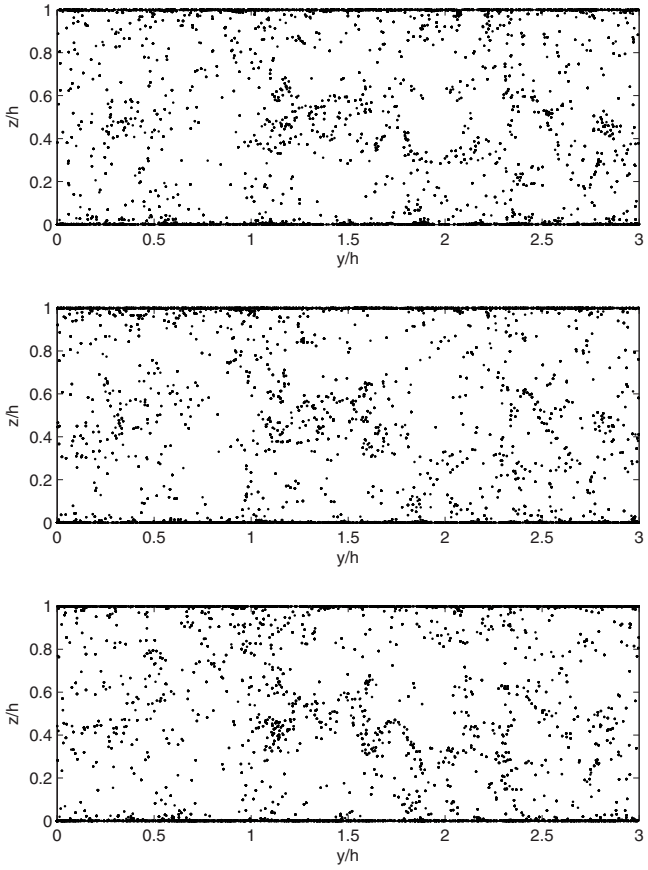

FIG. 7. Instantaneous distribution of particles around plane $x^+=720$ for particles of response time $\tau^+=30$. $\lambda=1$ (upper), $\lambda=3$ (middle), and $\lambda=10$ (lower).

initially confined inside an eddy will either stay inside the eddy or be thrown out. The whole process depends on the particle inertia. It is believed that the present particles have sufficient inertia to be centrifuged out of the structures and thereby end up in convergent zones or low-speed regions.

Contours of wall-normal fluid velocity in the cross-sectional plane at $x^+=720$ are shown in Fig. 5. Also here, the distribution of particles around the same plane is shown in Fig. 6 for $\tau^+=5$ particles and Fig. 7 for $\tau^+=30$ particles, respectively. The particles seem to cluster into groups leaving regions empty of particles behind. It is also evident that these particle-free regions, or voids, are located at the same places in the cross section for all three particle sets, i.e., irrespective of aspect ratio λ. Another feature which is visible from the figures is that many of the particle clusters seem to make an angle between 30° and 45° with the wall normal. This was observed by Marchioli and Soldati[6] for spherical particles and can be attributed to the turbulence structures.

Instantaneous ($t^+=5760$) streamwise vorticity contours at the plane $x^+=720$ are shown in Fig. 8. Close to the wall, at $z/h\approx 0.06$ or $z^+\approx 21$, two primary vortices of opposite polarity are seen. Figures 9 and 10 show the distribution of $\tau^+=5$ and $\tau^+=30$ particles in the same region, respectively. What is evident from the figures is that both the slow and the fast particles are absent close to the primary vortex cores. More of the faster particles seem to be present near the borders of the vortices. The slower particles are more numerous very close to the walls. In the lower right corner, $(y/h, z/h)\approx(0.53, 0.01)$, there is an accumulation of $\tau^+=30$ particles. This corresponds to a region of low-speed fluid velocity which arises due to streamwise vortices of opposite polarity (see Ref. 40).

B. Translational velocity statistics

To produce particle statistics, the computational domain is divided into 200 equal volumes with base area spanned by the streamwise and spanwise lengths of the computational domain. The volume heights equal $h/200$. In each volume,

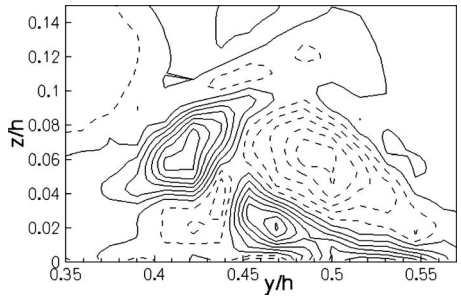

FIG. 8. Instantaneous contours of streamwise fluid vorticity at the plane $x^+=720$. The solid lines are positive and the dashed lines are negative velocity.

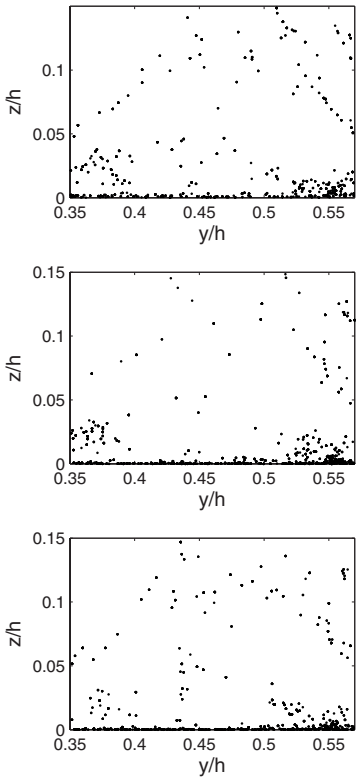

FIG. 9. Instantaneous distribution of particles around plane $x^+=720$ for particles of response time $\tau^+=5$. $\lambda=1$ (upper), $\lambda=3$ (middle), and $\lambda=10$ (lower).

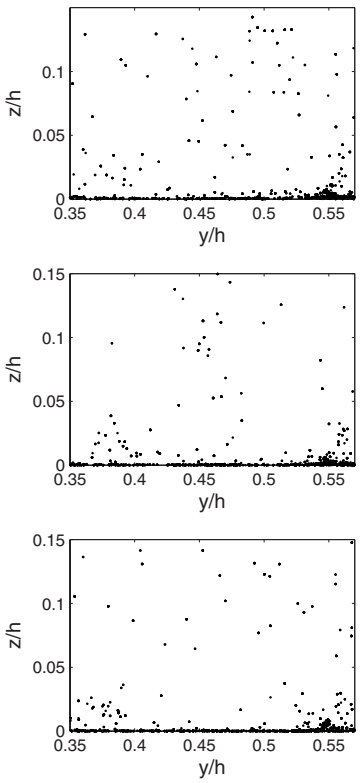

FIG. 10. Instantaneous distribution of particles around plane $x^+=720$ for particles of response time $\tau^+=30$. $\lambda=1$ (upper), $\lambda=3$ (middle), and $\lambda=10$ (lower).

the mean of a variable equals the sum of that variable for all particles divided by the number of particles in the volume. The statistics presented in this section is gathered over 80 000 timesteps or 2880 viscous time units.

The mean fluid and particle streamwise velocities are shown in Figs. 11 and 12 for $\tau^+=5$ and $\tau^+=30$ particles, respectively. Also, the conditionally averaged fluid velocities at the particle positions are shown. From Fig. 11(a), it is clear that the mean fluid velocity exceeds the corresponding particle velocities in the near-wall region. Away from the wall, i.e., beyond $z^+\approx 50$, the velocity profiles of the particles and the fluid collapse. There is hardly any differences between ellipsoids and spherical particles, except very close to the wall ($z^+<2$), where the velocity of the spherical particles exceeds that of the ellipsoids. It was seen in Fig. 3 that the same particles preferentially concentrated in low-speed fluid velocity regions. This can also be seen from Fig. 11(b). The conditionally averaged fluid velocities are clearly lagging the mean fluid velocity. Hence, the consequence of preferential concentration is a lowering of particle mean velocity compared to the fluid. On the other hand, the inertia of the fast particles is not large enough to cause any specific deviations between the mean particle velocity and the conditionally averaged fluid velocity. This is not the case for the slower $\tau^+=30$ particles, as can be seen from Figs. 12(a) and 12(b). In the near-wall region, $1<z^+<6$, the mean particle velocities exceed the corresponding fluid velocity. Also here, there is no pronounced difference between ellipsoidal and spherical particles. From Fig. 12(b) it is seen that the slow particles concentrate in regions of low streamwise fluid velocity. Due to their larger inertia, these particles will not respond fast enough to the local fluid environment, and hence retain a larger velocity than both the mean fluid and conditionally averaged fluid velocities. In the buffer layer, however, the mean particle velocity v_x is lower than the mean fluid velocity u_x, just as for the faster particles in Fig. 11. Several researchers have observed the decrease in mean particle velocity relative to the fluid velocity for spherical particles.[41,4,7] Kaftori *et al.*[4] experimentally observed that the average velocity of spherical particles was lower than the average fluid velocity. They claimed that this was due to the entrainment process, which is caused by funnel-shaped vortical structures. The present results show that ellipsoidal particles behave similarly.

The root-mean-square (rms) values of the fluctuating particle and fluid velocities are shown in Fig. 13(a) for $\tau^+=5$ particles. It is seen that the particle rms velocities exceed the corresponding fluid velocities in the streamwise direction, while they are lagging the fluid in the spanwise and wall-normal direction. There is hardly any effect of particle aspect ratio on the particle intensities in the spanwise and wall-normal directions. In the streamwise direction, the particle intensity is slightly increasing with increasing aspect ratio in the near-wall region. Figure 13(b) shows the conditionally averaged fluid rms velocities. By comparing Figs. 13(a) and 13(b), it is obvious the particle rms velocities are combined results of preferential concentration and particle inertia. Because of the mean fluid velocity gradient, the particles will have larger streamwise intensity locally than the

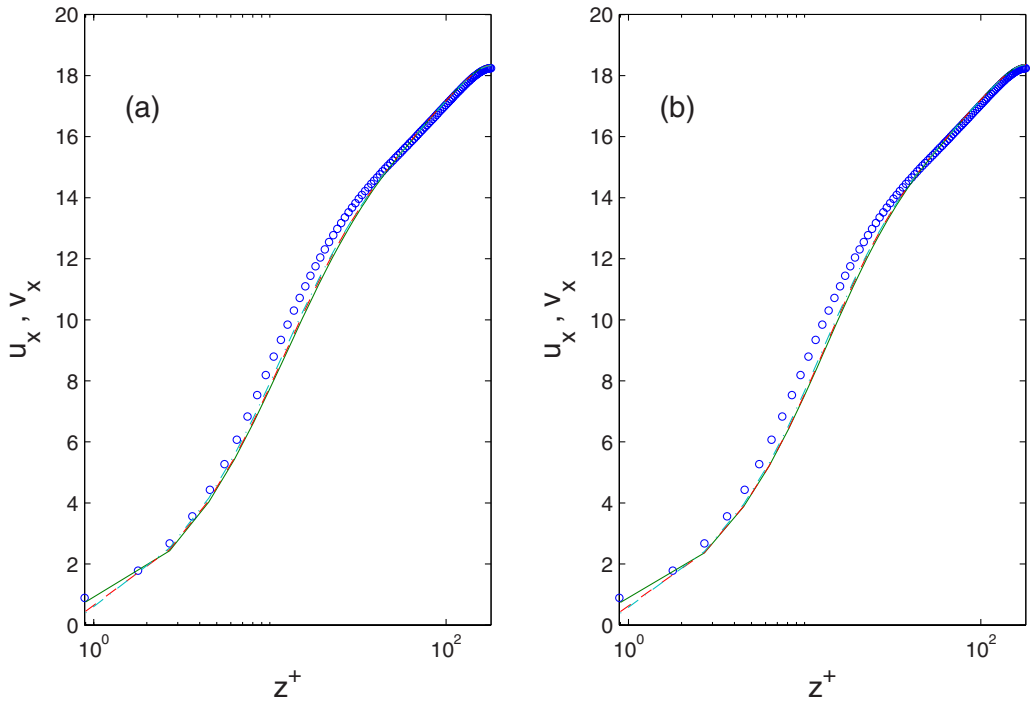

FIG. 11. (Color online) Mean fluid and particle velocities for $\tau^+=5$; (◯) fluid, (-) $\lambda=1$, (- -) $\lambda=3$, and (---) $\lambda=10$. (a) Particles; (b) conditionally averaged fluid. The three lines shown are nearly indistinguishable.

fluid (see, for instance, Refs. 42 and 2). On the other hand, the lack of mean velocity gradient in the spanwise and wall-normal directions will cause a reduction in particle intensities due to inertia in these directions. It should be remembered that the response time τ^+, defined in Eq. (11), is an equivalent response time. It is only exact for a spherical particle which is an isotropic body. The mass of an ellipsoidal particle is

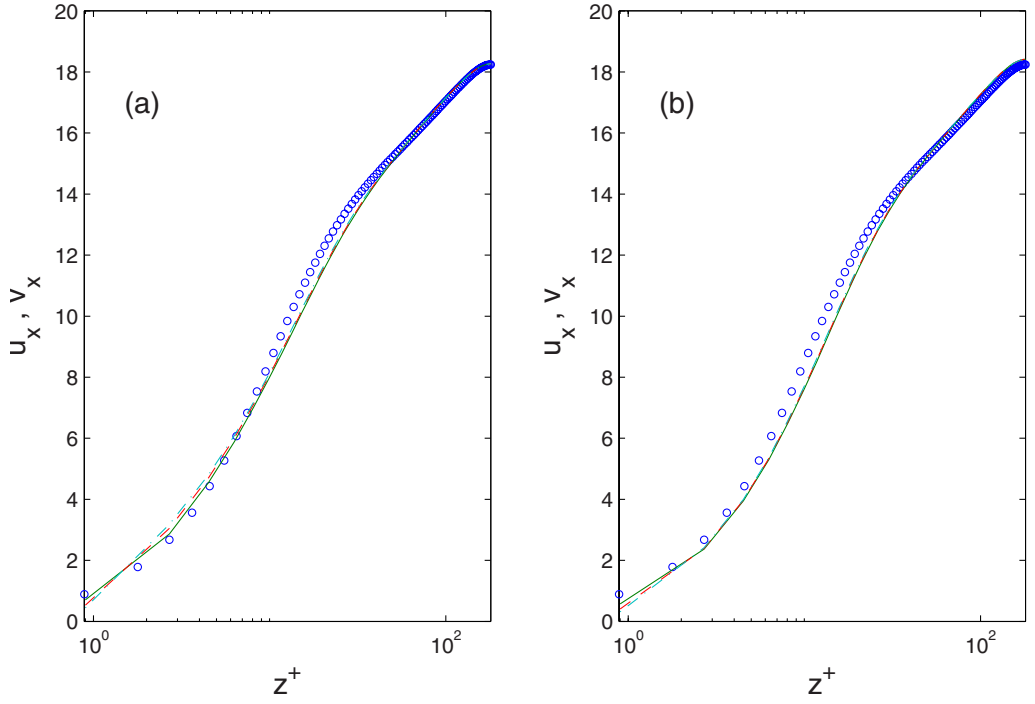

FIG. 12. (Color online) Mean fluid and particle velocities for $\tau^+=30$; (◯) fluid, (-) $\lambda=1$, (- -) $\lambda=3$, and (---) $\lambda=10$. (a) Particles; (b) conditionally averaged fluid. The three lines shown are nearly indistinguishable.

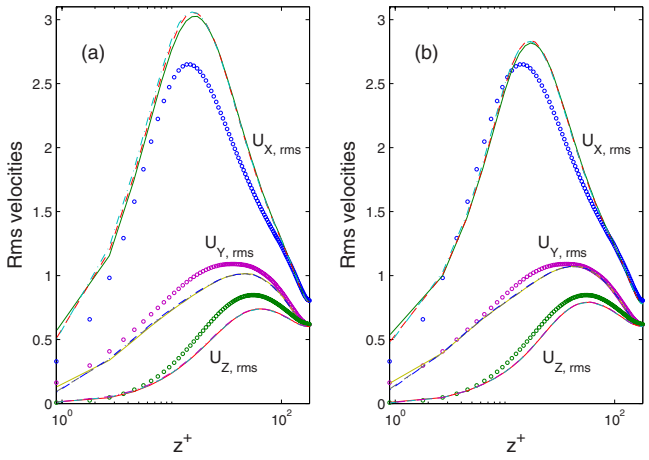

FIG. 13. (Color online) Streamwise rms velocity of fluid and particle for $\tau^+=5$; (o) fluid, (-) $\lambda=1$, (- -) $\lambda=3$, and (---) $\lambda=10$. (a) Particles; (b) conditionally averaged fluid. The data for the spheres ($\lambda=1$) are case B in Ref. 34.

$$m_e(\lambda) = \rho_p V_s \lambda, \tag{29}$$

where ρ_p is the particle density and V_s is the volume of a sphere with radius equal to the semiminor axis of the ellipsoid. Hence, from Table I is clear that

$$m_e(\lambda = 10) > m_e(\lambda = 3) > m_e(\lambda = 1). \tag{30}$$

This shows that the inertia of the particles increases with aspect ratio for a given τ^+ and explains the increase in streamwise intensity with aspect ratio. Figure 14 shows the same intensities, but for the slower $\tau^+=30$ particles. Here, it is seen that the deviations from the fluid intensities are even more pronounced, obviously due to larger particle inertia. The influence of preferential concentration, as seen from Fig. 14(b), remains about the same as for the faster particles in Fig. 13(b).

The mean relative streamwise velocity u_x-v_x is shown in Fig. 15. It is seen that the relative velocity is negative in the near-wall region. Also, as a consequence of particle inertia, this effect is most pronounced for the slower particles. For the faster particles [Fig. 15(a)], the minimum is at

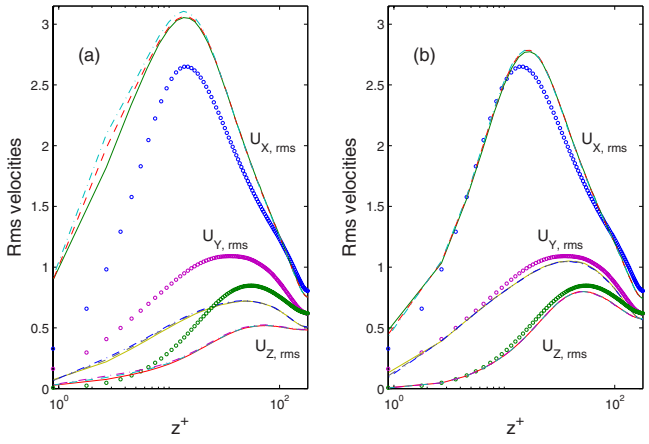

FIG. 14. (Color online) Streamwise rms velocity of fluid and particle for $\tau^+=30$; (◯) fluid, (-) $\lambda=1$, (- -) $\lambda=3$, and (---) $\lambda=10$. (a) Particles; (b) conditionally averaged fluid. The data for the spheres ($\lambda=1$) are case C in Ref. 34.

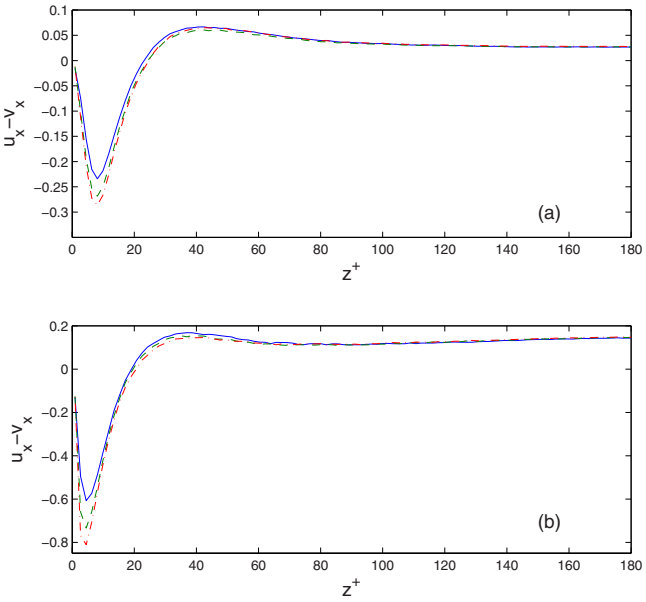

FIG. 15. (Color online) Mean streamwise relative velocity u_x-v_x; (-) $\lambda=1$, (- -) $\lambda=3$, and (---) $\lambda=10$. (a) $\tau^+=5$; (b) $\tau^+=30$.

$z^+\approx 10$, while the negative peak is shifted toward the wall for the slower particles [Fig. 15(b)]. For spherical particles, Kaftori *et al.*[4] observed this trend of negative streamwise slip velocity in their experiments. They explained that this was due to particle rotation, and that the superposition of translational and angular velocities resulted in larger particle velocities. Here, the rotational and translational particle velocities are not directly coupled (i.e., only indirectly coupled through particle orientation), yet the particles are traveling faster than the fluid. This effect also results in the mean velocity profiles in Figs. 11 and 12. Locally, the particles will on average travel faster than the fluid. The particles concentrate in low-speed regions, and the combination of both transverse and spanwise particle motions causes larger streamwise velocity on average due to particle inertia. Even though the particles may have a relatively large residence time in the low-speed streaks, the particle response time is mostly larger than the local timescale of the turbulence. Hence, the particles will retain their memory. As is also evident from Fig. 15, the negative relative velocity becomes even more negative with increasing aspect ratio for fixed response times. This is most likely an effect of increase in inertia, cf. Eq. (30). Away from the walls, the mean relative velocity becomes positive. In this region, the timescales of the flow are mostly larger than the particle response time, and the particles will respond promptly to the local fluid environment. The mean relative velocity of the ellipsoids becomes indistinguishable from that of the spheres.

C. Orientational statistics and spin

While the orientation of a spherical particle with respect to the flow field is dynamically irrelevant, the orientation of an ellipsoid does matter. Figure 16 shows a sketch of the three direction angles $(\theta_x,\theta_y,\theta_z)$ which define the orientation of the semimajor axis relative to the comoving frame $\mathbf{x}''$,

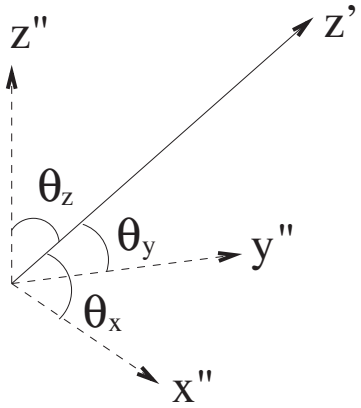

FIG. 16. Direction cosines.

which is always parallel to the inertial frame **x**; see Fig. 1. These angles will be used in the following to describe the orientational statistics of the ellipsoids.

The absolute values of the mean particle direction cosines (from now on called mean orientations) are shown in Fig. 17 for the ellipsoidal particles. The orientation of ellipsoidal particles is of general importance, since it influences the particle dynamics. It is seen from Figs. 17(a) and 17(b) that the ellipsoidal particles have preferential orientation in the streamwise direction. This was observed numerically by Zhang *et al.*[22] for small ellipsoidal particles of response time $\tau^+=2.26$ and aspect ratio $\lambda=5$ in the near-wall region (viscous sublayer, buffer layer). Newsom and Bruce[24] reported experimental results of horizontal orientation of fibrous aerosols in atmospheric turbulence. They found that fibers with larger diameters exhibited a greater tendency for horizontal orientation, i.e., the orientational preference was more sensitive to fiber diameter than to length. Here, the ellipsoidal diameter $2a$ is fixed and the length $2b$ is either $6a$ ($\lambda=3$) or $20a$ ($\lambda=10$). Hence, there is an increased orientation in the streamwise direction with aspect ratio for both particle response times. In a turbulent channel flow, the streamwise velocity fluctuations exceed the spanwise and wall-normal velocity fluctuations. It is believed that the streamwise fluid intensities contribute to a preferential streamwise orientation by aligning the particles in this direction. It is also observed that the faster particles are more oriented in the streamwise direction. This is an inertial effect. Slower particles are more resistant to turbulent velocity fluctuations. This can, for instance, be seen in Figs. 17(c) and 17(d), which show the spanwise orientation. The slower particles are less oriented in the spanwise direction as compared to the faster particles. The spanwise fluctuations are relatively weak, and if, for instance, a particle is oriented in the streamwise direction, it is harder to alter this orientation for a slow particle. It can be seen from Figs. 17(e) and 17(f) that the slower particles are more oriented toward the wall than the faster particles. One may speculate that the slower particles are mostly sensitive to streamwise fluctuations, although the present data do not provide direct support of this conjecture. As the velocity fluctuations bring the particles to a streamwise orientation,

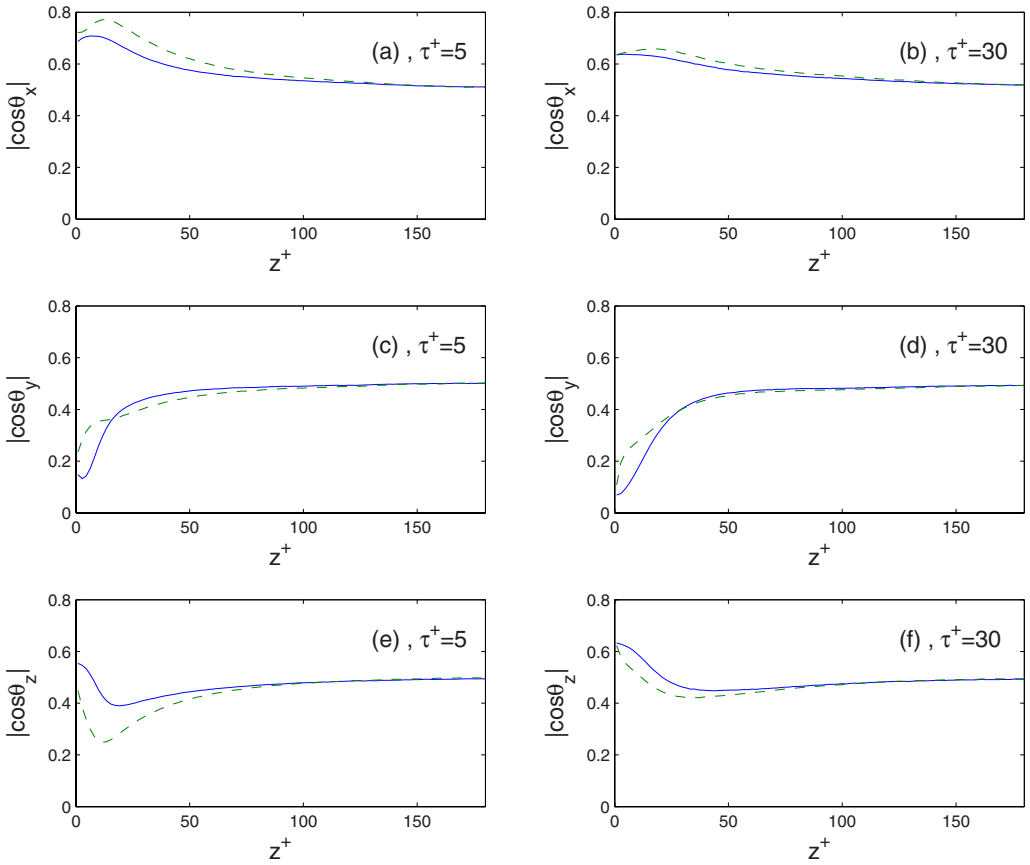

FIG. 17. (Color online) Absolute values of mean direction cosines; (-) $\lambda=3$; (- -) $\lambda=10$. [(a) and (b)] $|\cos\theta_x|$, [(c) and (d)] $|\cos\theta_y|$, and [(e) and (f)] $|\cos\theta_z|$.

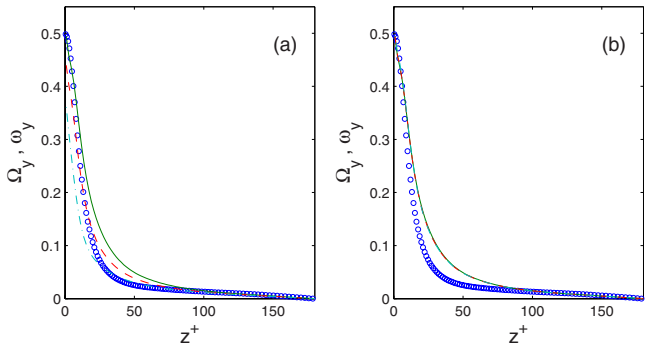

FIG. 18. (Color online) Mean spanwise spin for $\tau^+=5$; (◯) fluid, (-) $\lambda=1$, (- -) $\lambda=3$, and (---) $\lambda=10$. (a) Particles; (b) conditionally averaged fluid. The data for the spheres ($\lambda=1$) are case B in Ref. 34.

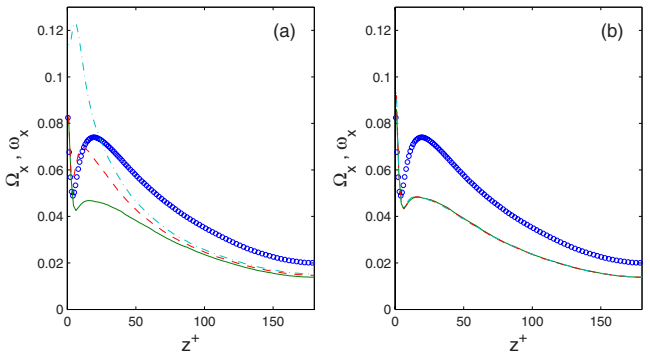

FIG. 20. (Color online) rms streamwise spin for $\tau^+=5$; (◯) fluid, (-) $\lambda=1$, (- -) $\lambda=3$, and (---) $\lambda=10$. (a) Particles; (b) conditionally averaged fluid. The data for the spheres ($\lambda=1$) are case B in Ref. 34.

the mean velocity gradient will be more effective in rotating the particles about the spanwise direction. Hence, the particle major axis is mostly confined to the *xz*-plane, and this is more pronounced for the slower particles.

The mean spanwise particle and fluid angular velocities, or spin, are shown in Figs. 18 and 19 for $\tau^+=5$ and $\tau^+=30$ particles, respectively. It is seen that the particles concentrate in regions of relatively large spanwise fluid spin [Figs. 18(b) and 19(b)], and this tendency is stronger for $\tau^+=5$ particles. Also, it seen that the rotational inertia of the spherical particles is not sufficient to cause any significant deviations from the conditionally averaged fluid spin at the spherical particle positions. Hence, the spanwise spin of spherical particles exceeds the corresponding fluid spin in the near-wall region. This has been shown numerically by Mortensen *et al.*,[34] while Ye and Roco[43] experimentally investigated the rotation of spherical particles in a Couette flow. They found that the particles' angular velocity was larger than the mean strain rate of the velocity field in the core of the flow. However, the mean spanwise spin of the ellipsoids is lower than that of the conditionally averaged fluid spin. This is surely an effect of rotational inertia. For a spherical particle, the rotational response time is defined as[9]

$$\tau_r^+ = \frac{Da^{+2}}{15\nu}. \tag{31}$$

This rotational response time is independent of direction due to the isotropic nature of a sphere. For an ellipsoidal particle, which is nonisotropic, the rotational response to the local flow field is much more complex. As far as the authors are aware of no such response time for ellipsoidal particles exists. From Eqs. (12)–(14) and (16)–(18), one could define at least two different response times for rotation about the x'-axis, which would appear in front of the rate-of-strain coefficients and the relative angular velocity between the fluid and particles. For both $\tau^+=5$ and $\tau^+=30$ particles, it is seen that mean spanwise particle spin in the near-wall region decreases with increasing aspect ratio. It can also be observed that the mean spanwise spin of the slower ellipsoids is larger than the corresponding spin of the faster ellipsoids. This also reflects the fact that the slower particles are more aligned in the *xz*-plane relative to the faster ones, as was seen in Fig. 17.

The fluctuating streamwise angular velocity components for $\tau^+=5$ and $\tau^+=30$ particles are shown in Figs. 20 and 21, respectively. Also shown is the conditionally averaged streamwise angular velocity intensities. It is seen that the particles avoid regions of large streamwise vorticity, and this is more pronounced for the faster $\tau^+=5$ particles. This is consistent with the instantaneous particle distribution in

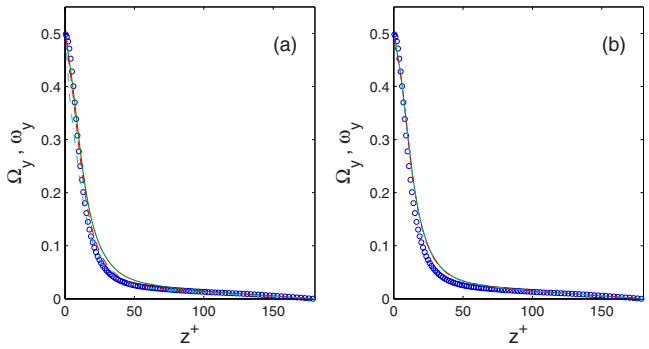

FIG. 19. (Color online) Mean spanwise spin for $\tau^+=30$; (◯) fluid, (-) $\lambda=1$, (- -) $\lambda=3$, and (---) $\lambda=10$. (a) Particles; (b) conditionally averaged fluid. The data for the spheres ($\lambda=1$) are case C in Ref. 34.

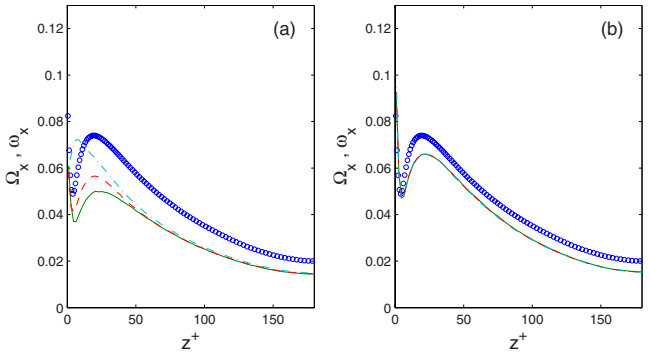

FIG. 21. (Color online) rms streamwise spin for $\tau^+=30$; (◯) fluid, (-) $\lambda=1$, (- -) $\lambda=3$, and (---) $\lambda=10$. (a) Particles; (b) conditionally averaged fluid. The data for the spheres ($\lambda=1$) are case C in Ref. 34.

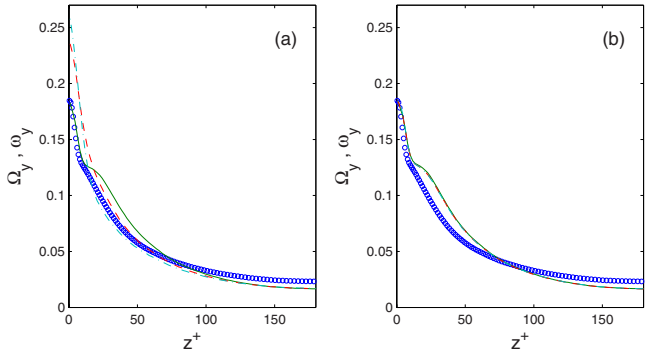

FIG. 22. (Color online) rms spanwise spin for $\tau^+=5$; (◯) fluid, (-) $\lambda=1$, (- -) $\lambda=3$, and (---) $\lambda=10$. (a) Particles; (b) conditionally averaged fluid. The data for the spheres ($\lambda=1$) are case B in Ref. 34.

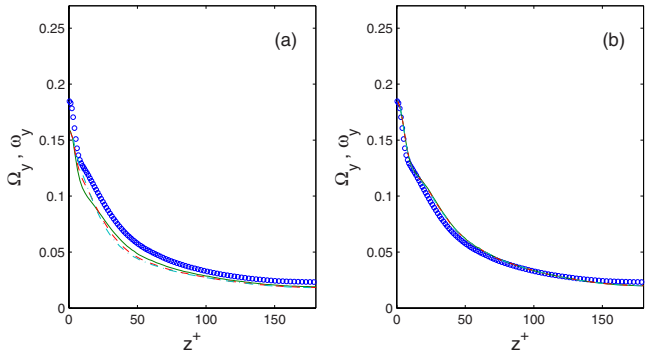

FIG. 23. (Color online) rms spanwise spin for $\tau^+=30$; (◯) fluid, (-) $\lambda=1$, (- -) $\lambda=3$, and (---) $\lambda=10$. (a) Particles; (b) conditionally averaged fluid. The data for the spheres ($\lambda=1$) are case C in Ref. 34.

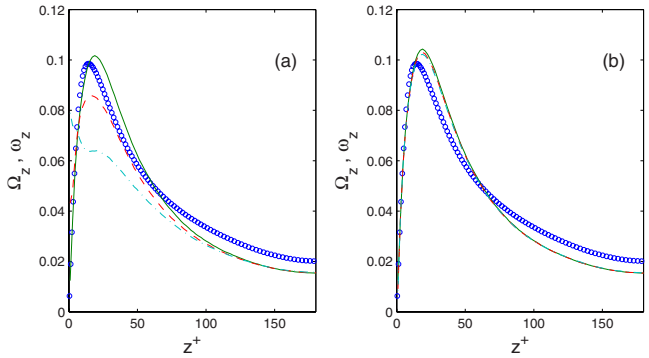

FIG. 24. (Color online) rms wall-normal spin for $\tau^+=5$; (◯) fluid, (-) $\lambda=1$, (- -) $\lambda=3$, and (---) $\lambda=10$. (a) Particles; (b) conditionally averaged fluid. The data for the spheres ($\lambda=1$) are case B in Ref. 34.

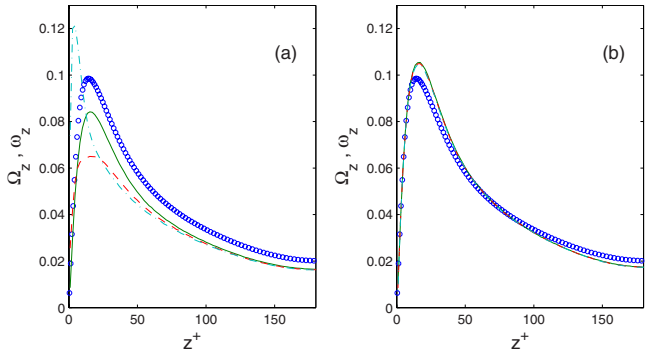

FIG. 25. (Color online) rms wall-normal spin for $\tau^+=30$; (◯) fluid, (-) $\lambda=1$, (- -) $\lambda=3$, and (---) $\lambda=10$. (a) Particles; (b) conditionally averaged fluid. The data for the spheres ($\lambda=1$) are case C in Ref. 34.

Figs. 9 and 10. The ellipsoids and spheres seem to concentrate in the same flow regions. However, rotational inertia causes large deviations between the particle intensities and the conditionally averaged intensities, except for $\tau^+=5$ spherical particles. There are clearly differences in the streamwise spin intensities between the ellipsoids and the spheres. This is most evident from Fig. 20(a). In both figures, it is seen that the spin intensities increase with aspect ratio. Figure 17 showed that the effect of increased aspect ratio was to promote the particle orientation in the mean flow direction. It was believed that the fluid velocity fluctuations were more effective in altering the orientation of the faster particles. The same effect may also lead to larger fluctuations in streamwise spin intensities.

Figures 22 and 23 show the spanwise spin intensities of $\tau^+=5$ and $\tau^+=30$ particles. It is seen that the particle spin intensities fall below that of the conditionally averaged fluid spin, except for the ellipsoids of response time $\tau^+=5$ in the near-wall region ($z^+<15$). There is hardly any differences between the particle intensities for the slowest particles. This tells that slower ellipsoidal particles are mostly aligned with the *xz*-plane. Also, rotational inertia is effective in damping the intensities as compared to the fluid. However, this is not the case for $\tau^+=5$ ellipsoids in the near-wall region. Also here it is believed that the fluid intensities affect the orientational behavior of the ellipsoids and hence the spanwise spin intensities.

The wall-normal spin intensities of the particles and the fluid are shown in Figs. 24 and 25, respectively. Again, it is seen that the conditionally averaged fluid profiles basically collapse for the different particles, which reflects that ellipsoids and spheres concentrate in the same flow regions. For the fastest spherical particles, there is no difference between particle spin intensities and the conditionally averaged fluid spin intensities. For the $\tau^+=30$ spherical particles, rotational inertia is effective in bringing the particle spin below the fluid spin. However, rotational inertia is even more dominating on ellipsoids of aspect ratio $\lambda=3$. For both the fast and slow particles, the wall-normal particle spin intensities lag the corresponding fluid spin intensities. This is also the case for the ellipsoids of aspect ratio $\lambda=10$ and response time $\tau^+=5$, except very close to the wall where ellipsoids wall-normal spin exceeds the fluid spin and that of the other particles. This region is even broader for the slower $\lambda=10$ ellipsoids.

V. CONCLUSIONS

The dynamics of prolate ellipsoids in a directly simulated channel flow has been examined. The Reynolds number was 360, i.e., somewhat higher than $\mathrm{Re}_*=250$ as considered in Ref. 22. The computational domain was three times longer and 50% wider than that used by Zhang *et al.*[22] in order to accommodate the largest scales of the turbulence. The ellipsoids were assumed to be small and the coupling between the fluid and the particles was one way. The ellipsoidal particles were affected both by inertia and hydrodynamic forces and torques, and the particle orientation became an essential ingredient in the adopted Largrangian approach. Simulations

were performed for three different particle aspect ratios and two different particle response times. In order to enable accurate particle statistics, equations of translational and rotational motions and orientations were integrated for 1 000 000 particles of each of the six categories.

The present simulations were consistently based on the assumption of Stokes flow conditions. The authors are not aware of any nonlinear extensions to the linear drag force (6) and the linear torque (16)–(18) for ellipsoidal particles. For spherical particles, however, the nonlinear drag formula (28) was used, for instance, by Kuerten.[37] The particle Reynolds number can be expressed in inner variables as $\mathrm{Re}_p = 2|u^+ - v^+|a^+$. The particle relative velocity $|u^+ - v^+|$ is consistently below unity and of the order of 0.1 outside the viscous-affected near-wall layer, i.e., beyond $z^+ \approx 20$ (see Fig. 15). All particle classes considered herein have the same $a^+ = 0.36$ and Re_p does therefore not exceed unity. A comparison with the results of Kuerten[37] showed that they were indistinguishable from the present results for the fastest spheres (case F1: $\tau^+ = 5$; $\lambda = 1$) obtained with Stokes drag, whereas the streamwise particle intensities for the slower spheres (case S1: $\tau^+ = 30$; $\lambda = 1$) slightly exceeded those observed by Kuerten[37] only in the innermost wall layer, i.e., for $z^+ < 10$. Although the effect of nonlinear drag is practically negligible for spherical particles in the present parameter range, the slip velocity $|u^+ - v^+|$ tends to increase with increasing particle aspect ratio λ and nonlinear effects might therefore be influential even for moderately slow particles.

The translational motion of the ellipsoidal particles was practically unaffected by the aspect ratio. The magnitude of the drift velocity, however, increased with λ in the buffer region and this is believed to be due to particle inertia. In the logarithmic layer and further out, the aspect ratio lost its significance.

Both ellipsoids and spheres accumulated in the viscous sublayer and preferentially concentrated in low-speed streaks. This phenomenon is well known for spherical particles and was also observed for ellipsoids by Zhang *et al.*[22] In the present study it was also observed that the ellipsoids and spheres tended to cluster in regions with strong wallward flow.

The tendency observed by Zhang *et al.*[22] of the ellipsoids to orient in mean flow direction was confirmed by the present simulations. We found that this tendency was most pronounced for the faster particles with the largest aspect ratio. The lateral tilting of the slower ellipsoids was suppressed in the viscous sublayer and their orientation was accordingly confined to the vertical xz-plane. This phenomenon was interpreted as a combined effect of mean shear and fluid velocity fluctuations.

While the translational motion was practically unaffected by the particle aspect ratio, both mean and fluctuating spin components depended crucially on λ. The mean spanwise particle spin, which was greater than the mean fluid spin in the near-wall region, turned out to diminish with increasing λ, and this reduction was ascribed to rotational inertia. Zhang *et al.*[22] observed that the ellipsoidal particles mostly rotated about the spanwise axis due to the mean shear field with little rotation about the wall-normal axis. These general findings are consistent with the results of this study. The present investigation revealed that while the fluctuating spanwise spin component is only modestly affected by the aspect ratio, the two other spin components are crucially dependent on λ. This behavior is not due to the distinct preferential particle concentration but is a direct effect of rotational inertia.

ACKNOWLEDGMENTS

This work has been supported by The Research Council of Norway through the PETROMAKS program. The authors would like to thank Professor G. Ahmadi for helpful electronic mail conversations and Dr. Roar Meland.

[1] J. B. McLaughlin, "Aerosol particle deposition in numerically simulated channel flow," Int. J. Multiphase Flow **1**, 1211 (1989).
[2] J. D. Kulick, J. R. Fessler, and J. K. Eaton, "Particle response and turbulence modification in fully developed channel flow," J. Fluid Mech. **277**, 109 (1994).
[3] D. Kaftori, G. Hetsroni, and S. Banerjee, "Particle behavior in the turbulent boundary layer. I. Motion, deposition, and entrainment," Phys. Fluids **7**, 1095 (1995).
[4] D. Kaftori, G. Hetsroni, and S. Banerjee, "Particle behavior in the turbulent boundary layer. II. Velocity and distribution profiles," Phys. Fluids **7**, 1107 (1995).
[5] Y. Pan and S. Banerjee, "Numerical simulation of particle interactions with wall turbulence," Phys. Fluids **8**, 2733 (1996).
[6] C. Marchioli and A. Soldati, "Mechanisms for particle transfer and segregation in a turbulent boundary layer," J. Fluid Mech. **468**, 283 (2002).
[7] C. Marchioli, M. Picciotto, and A. Soldati, "Influence of gravity and lift on particle velocity statistics and transfer rates in turbulent vertical channel flow," Int. J. Multiphase Flow **33**, 227 (2007).
[8] G. B. Jeffery, "The motion of ellipsoidal particles immersed in a viscous fluid," Proc. R. Soc. London, Ser. A **102**, 161 (1922).
[9] H. Brenner, "The Stokes resistance of an arbitrary particle," Chem. Eng. Sci. **18**, 1 (1963).
[10] H. Brenner, "The Stokes resistance of an arbitrary particle-II: An extension," Chem. Eng. Sci. **19**, 599 (1964).
[11] H. Brenner, "The Stokes resistance of an arbitrary particle-III: Shear fields," Chem. Eng. Sci. **19**, 631 (1964).
[12] H. Brenner, "The Stokes resistance of an arbitrary particle-IV: Arbitrary fields of flow," Chem. Eng. Sci. **19**, 703 (1964).
[13] H. Brenner, "The Stokes resistance of an arbitrary particle-V: Symbolic operator representation of intrinsic resistance," Chem. Eng. Sci. **21**, 97 (1966).
[14] J. Happel and H. Brenner, *Low Reynolds Number Hydrodynamics with Special Applications to Particulate Media*, 2nd ed. (Martinus Nijhoff, The Hague, 1983).
[15] E. Y. Harper and I. D. Chang, "Maximum dissipation resulting from lift in a slow viscous shear flow," J. Fluid Mech. **33**, 209 (1968).
[16] J. Lin, X. Shi, and Z. Yu, "The motion of fibers in an evolving mixing layer," Int. J. Multiphase Flow **29**, 1355 (2003).
[17] F. G. Fan and G. Ahmadi, "Dispersion of ellipsoidal particle in an isotropic pseudo-turbulent flow field," J. Fluids Eng. **117**, 154 (1995).
[18] J. A. Olson, "The motion of fibres in turbulent flow, stochastic simulation of isotropic homogeneous turbulence," Int. J. Multiphase Flow **27**, 2083 (2001).
[19] M. Shapiro and M. Goldenberg, "Deposition of glass fiber particles from turbulent air flow in a pipe," J. Aerosol Sci. **24**, 65 (1993).
[20] F. G. Fan and G. Ahmadi, "A sublayer model for turbulent deposition of particles in vertical ducts with smooth and rough surfaces," J. Aerosol Sci. **24**, 45 (1993).
[21] F. G. Fan and G. Ahmadi, "A sublayer model for wall-deposition of ellipsoidal particles in turbulent streams," J. Aerosol Sci. **26**, 813 (1995).
[22] H. Zhang, G. Ahmadi, F. G. Fan, and J. B. McLaughlin, "Ellipsoidal particles transport and deposition in turbulent channel flows," Int. J. Multiphase Flow **27**, 971 (2001).
[23] J. D. Klett, "Orientation model for particles in turbulence," J. Atmos. Sci. **52**, 2276 (1995).
[24] R. K. Newsom and C. W. Bruce, "Orientational properties of fibrous aero-

sols in atmospheric turbulence," J. Aerosol Sci. **29**, 773 (1998).
[25]J. Lin, W. Zhang, and Z. Yu, "Numerical research on the orientation distribution of fibers immersed in laminar and turbulent pipe," J. Aerosol Sci. **35**, 63 (2004).
[26]M. Manhart, "Rheology of suspensions of rigid-rod like particles in turbulent channel flow," J. Non-Newtonian Fluid Mech. **112**, 269 (2003).
[27]J. S. Paschkewitz, Y. Dubief, C. D. Dimitropoulos, E. S. G. Shaqfeh, and P. Moin, "Numerical simulation of turbulent drag reduction using rigid fibers," J. Fluid Mech. **518**, 281 (2004).
[28]J. J. J. Gillissen, B. J. Boersma, P. H. Mortensen, and H. I. Andersson, "On the performance of the moment approximation for the numerical computation of fiber stress in turbulent channel flow," Phys. Fluids **19**, 035102 (2007).
[29]H. Goldstein, *Classical Mechanics*, 2nd ed. (Addison-Wesley, Reading, 1980).
[30]P. H. Mortensen, H. I. Andersson, J. J. J. Gillissen, and B. J. Boersma, "On the motion of ellipsoidal particles suspended in a turbulent channel flow," *Proceeding of the Fifth International Symposium On Turbulence, Heat and Mass Transfer* (Begell House, Wallingford, 2006), p. 683.
[31]I. Gallily and A. H. Cohen, "On the orderly nature of the motion of nonspherical aerosol particles. II. Inertial collision between a spherical large droplet and axially symmetrical elongated particle," J. Colloid Interface Sci. **68**, 338 (1979).
[32]M. P. Allan and D. J. Tildesley, *Computer Simulation of Liquids* (Oxford University Press, Oxford, 1988).
[33]B. Arcen, A. Tanière, and B. Osterlè, "On the influence of near-wall forces in particle laden channel flows," Int. J. Multiphase Flow **32**, 1326 (2006).
[34]P. H. Mortensen, H. I. Andersson, J. J. J. Gillissen, and B. J. Boersma, "Particle spin in a turbulent channel flow," Phys. Fluids **19**, 078109 (2007).
[35]S. Elghobashi, "On predicting particle-laden turbulent flows," Appl. Sci. Res. **52**, 309 (1994).
[36]J. G. M. Kuerten and A. W. Vreman, "Can turbophoresis be predicted by large-eddy simulation?" Phys. Fluids **17**, 011701 (2005).
[37]J. G. M. Kuerten, "Subgrid modeling in particle-laden channel flow," Phys. Fluids **18**, 025108 (2006).
[38]S. K. Robinson, "Coherent motions in the turbulent boundary layer," Annu. Rev. Fluid Mech. **23**, 601 (1991).
[39]J. K. Eaton and J. R. Fessler, "Preferential concentration of particles by turbulence," Int. J. Multiphase Flow **20**, 169 (1994).
[40]P. A. Davidson, *Turbulence: An Introduction for Scientists and Engineers* (Oxford University Press, Oxford, 2004).
[41]M. Rashidi, G. Hetsroni, and S. Banarjee, "Particle-turbulence interaction in a boundary layer," Int. J. Multiphase Flow **16**, 935 (1990).
[42]L. M. Liljegren, "The effect of a mean fluid velocity gradient on the streamwise velocity variance of a particle suspended in a turbulent flow," Int. J. Multiphase Flow **19**, 471 (1993).
[43]J. Ye and M. C. Roco, "Particle rotation in Couette flow," Phys. Fluids A **4**, 220 (1992).